



Markov random field-based image inpainting with direction structure distribution analysis for maintaining structure coherence



Jixiang Cheng, Zhidan Li*

School of Electrical Engineering and Information, Southwest Petroleum University, Chengdu 610500, PR China

ARTICLE INFO

Article history:

Received 2 April 2018

Revised 4 August 2018

Accepted 3 September 2018

Available online 5 September 2018

Keywords:

Image inpainting

Structure coherence

Markov random field

Direction structure distribution analysis

Desired direction structures

ABSTRACT

Image inpainting provides a means for restoration of an image with some damaged portions and has been widely applied to many fields. However, many existing inpainting methods still suffer the difficulties of effectively and efficiently maintaining structure coherence. To tackle the problems, this paper proposes a direction structure distribution analysis strategy for Markov Random Field (MRF)-based image inpainting algorithms. In the strategy, the desired direction structures (DDS) are selected and applied to guide the inpainting process. Given a degraded image, four kinds of direction edge information are extracted by super-wavelet transform, canny and dilation operators. Then local direction edge gradient magnitude is applied for direction structure distribution analysis and DDS are selected according to gradient variance. Afterwards, offsets of similar patches are calculated and only a few dominated offsets are chosen as candidate offsets. Finally, graph-cut optimization technology is utilized to solve energy function. Experimental results show that the proposed method achieves generally better performance than nine state-of-the-art methods in terms of the abilities of maintaining structure coherence and the computational cost on inpainting different kinds of degraded images.

© 2018 Elsevier B.V. All rights reserved.

1. Introduction

Image inpainting, also called image completion or image restoration, was originally proposed by Bertalmio, et, al. [4] to recover the missing region of an image using the information extracted from the known region of the image. Generally, the inpainted image should possess patterns consistent with the known region so that the inpainting trail can not be easily observed. Nowadays, image inpainting has become an active research subject of computer vision and image processing. Many techniques with unique features have been devised by mathematicians or computer scientists, and the applications of image inpainting are extensive, such as old photos and damaged films restoration, art conservation and restoration, and texts or objects removal from images [6].

Image inpainting methods can be classified into four categories: diffusion-based methods, sparse-based methods, exemplar-based methods, and deep learning based methods. The diffusion-based methods, focusing on filling narrow or small holes, adopt diffusion systems to diffuse image information from source region into missing region. Several partial differential equations (PDEs) have been used to infer diffusion information, such as Navier-Stokes equations

[3], Euler-Lagrange equations [56], third-order PDEs [9], fourth-order PDEs [29], Mumford Shah model [46], and multichannel nonlocal total variation model [10]. In [44,45], the neighborhood pixels are utilized to interpolate the missing pixels. Due to the lack of semantic texture or structure synthesis, diffusion-based methods perform poorly on inpainting images with small structure or texture missing region.

The sparsity-based methods, also suitable for filling small missing region, adopt sparse representation to complete degraded images. In [16,17,22,49], super-wavelet was applied to reconstruct incomplete images. In [7,8,32], based on wavelet transform, whole energy constraint optimization equation was constructed to infer missing information. As the basis of wavelet or super-wavelet transform are fixed, dictionary learning methods were devised to enhance the generalization of the methods, such as [15,31]. In recent years, matrix completion methods were devised for image inpainting task, where low-rank matrix factorization [13,37,51] and deep learning [18] were adopted to infer missing region. Similar to diffusion-based methods, sparsity-based methods may fail to recover structures and textures when dealing with large missing region.

The exemplar-based methods propagate information from source region into missing region at patch level. Compared with the former two kinds of methods, exemplar-based methods perform more effectively when filling large hole [12]. This kind of

* Corresponding author.

E-mail addresses: chengjixiang0106@126.com (J. Cheng), dan.807@163.com (Z. Li).

methods can be further divided into matching-based methods and Markov Random Field (MRF)-based methods. For the first category, the key steps include two procedures, i.e., filling order determination and patch selection. In [52,55], structure sparsity function and color distribution were utilized to determine filling order. In [30], the completion order was determined through color texture and curvature features. In [47,48], a space varying updating strategy and a regularized factor were proposed to improve filling priority estimation, respectively. In our previous work [33], color-direction structure sparsity function was defined to obtain robust filling order by simultaneously considering direction feature and color distribution. In [12,19,35,55], several match criteria were defined to implement patch selection. To reduce block effect and seam effect, linear combination or sparse representation of several candidate patches was adopted to fill missing region [11,21,33,34,52]. However, the error may propagate in subsequent filling procedure. In addition, the matching-based methods are computational expensive.

MRF-based methods formulate image inpainting as a discrete MRF optimization problem [6,23,27,36,43]. In the methods, the known pixel/patch and the missing pixel/patch are respectively regarded as a label and a node, and the problem becomes assigning a suitable label to a node, which can be solved by belief propagation [28], priority belief propagation [20,41], graph-cuts [40], or their variants [5,28,38]. To obtain appropriate labels and reduce time-complexity, He and Sun [24,53] selected a few dominant offsets to calculate the extreme of whole energy. Liu and Caselles [36] used nearby offsets and multi-scale policy to solve energy function. However, these methods would not well maintain the structure coherence of inpainted results when the known region does not contain enough desired structures, that is, the selected offsets are not the desired offsets. Thus, whether the offsets is suitable or not is quite important for obtaining pleasant inpainting results.

As a new branch of artificial intelligence, deep learning has attracted attentions from various fields including image inpainting. In [1], missing regions was first determined by regression analysis and then general regression neural network was applied to repair damaged pixels. In [39], a convolutional neural network named context encoder was trained to generate the contents of an image conditioned on its surroundings. In [26], a fully-convolutional neural network with the help of global and local context discriminators was applied to fill in missing region of any shape. In [54], the missing content was inferred by a trained deep generative model with context and prior losses. Deep learning have produced competitive inpainting results, however, it requires huge computation power and a large number of sample images, which may limits its applications.

Human eye is sensitive to the loss of high frequency information, such as edge, corner and structure. Therefore, structure coherence should be highly regarded and several work has been done particulary for maintaining structure coherence. In [27], adaptive ND tensor voting was proposed to infer missing information, which is suitable for images consisting of roughly homogeneous and periodic textures. In [43], a few curves or lines were firstly specified by users in order to propagate structure and then applied to synthesize texture. However, the method requires human interference which may limits its application. In [2], random sampling was utilized to find good matches and the matches were propagated to surrounding areas according to natural coherence. In [30], an inpainting approach including salient structure completion and texture propagation was proposed. In [14], image melding process was proposed for filling holes through integrating image gradient into patch representation and a new energy function. In [24], patch offset statistics being able to capture distribution feature of images were applied to guide inpainting process. In [25], mid-level struc-

tural cues were utilized for inpainting task, where planar structure was defined to find patch offsets in different planes depending on translation regularity. In [41], contextual descriptors were employed to guide inpainting process. In [20], patch selection from groups of similar patches and optimal patch assignment through joint patch refinement were applied to improve inpainting performance. These works improve structure coherence for some cases in a certain degree. However, when inpainting images with few known structures, these methods do not work effectively. To address this problem, this paper proposes a novel direction structure distribution analysis strategy for MRF-based methods in order to better maintain structure coherence especially for images with few known structures. With this strategy, a few candidate offsets that can improve structure coherence are elaborately selected out according to the characteristics of neighboring regions of the target region. Specifically, for a given degraded image, edge information of four directions (i.e., 0°, 45°, 90°, and 135°) is first extracted by super-wavelet transform [42], canny and dilation operators. Then gradient is applied to describe the intensity of different direction structures and gradient variance is utilized to measure the direction structure distribution. On this basis, DDS are selected. Afterwards, for desired direction and non-direction offsets, only a few dominated offsets are chosen as candidate offsets. Finally, the graph-cuts [5] is adopted to solve energy function. Experimental results show that the proposed method outperforms nine state-of-the-art approaches on inpainting several kinds of degraded images. Meanwhile, the computation time of the proposed method is satisfactory, much less than some of compared methods.

The rest of this paper is organized as follows. Section 2 presents the framework of MRF-based methods as well as the motivation of the work. Section 3 details the proposed direction structure distribution analysis strategy for MRF-based methods, including direction feature extraction, desired structure feature selection, candidate offsets selection, and a brief analysis of the proposed method. Section 4 presents the experimental results on a variety of images, which demonstrates the superiority over nine state-of-the-art methods. Conclusions are made in Section 5.

2. Framework of MRF-based methods

Given a degraded image I with missing region Ω , a pixel p located at the position $\mathbf{x} = (x, y)$ in the missing region is filled with a certain pixel q located at the position $\mathbf{x} + \mathbf{s}$ from the known region, where $\mathbf{s} = (u, v)$ is the offset. Therefore, the inpainting problem is how to assign a suitable offset \mathbf{s} to each unknown pixel at \mathbf{x} . Given the offsets, the inpainted image can be obtained by combining a stack of shifted images corresponding to these offsets. In MRF-based methods, the known pixel/patch and the missing pixel/patch are regarded as label and node, and how to assign the labels or offsets is implemented by minimizing the following energy function:

$$E(L) = \sum_{\mathbf{x} \in \Omega} E_d(L(\mathbf{x})) + \sum_{\mathbf{x}, \mathbf{x}' \in \Omega} E_s(L(\mathbf{x}), L(\mathbf{x}')), \quad (1)$$

where the neighboring pixels (\mathbf{x} , \mathbf{x}') are 4-connected; the argument L is a labeling map which assigns a label from a pre-selected offsets $\{\mathbf{s}_i\}$ to the unknown pixel at position \mathbf{x} , e.g., $L(\mathbf{x}) = i$ means the missing pixel at \mathbf{x} is filled with the pixel at $\mathbf{x} + \mathbf{s}_i$. The data term E_d is 0 if the label is valid for \mathbf{x} , i.e., $\mathbf{x} + \mathbf{s}$ locates at the known region; otherwise E_d is $+\infty$. Denoting $a = L(\mathbf{x})$ and $b = L(\mathbf{x}')$, the smooth term E_s is defined as:

$$E_s(a, b) = \|I(\mathbf{x} + \mathbf{s}_a) - I(\mathbf{x} + \mathbf{s}_b)\|^2 + \|I(\mathbf{x}' + \mathbf{s}_a) - I(\mathbf{x}' + \mathbf{s}_b)\|^2, \quad (2)$$

where $I(\mathbf{x})$ is the RGB color value of \mathbf{x} ; $I(\cdot + \mathbf{s})$ is an image shifted by \mathbf{s} . If $\mathbf{s}_a \neq \mathbf{s}_b$, the neighboring pixels \mathbf{x} and \mathbf{x}' will be assigned

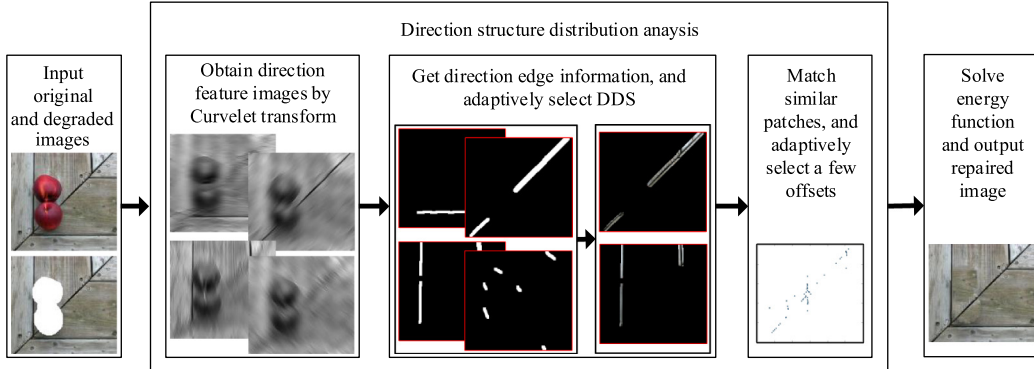


Fig. 1. The frame diagram of direction structure distribution analysis for MRF-based methods.

different labels, resulting a seam between \mathbf{x} and \mathbf{x}' . Hence, (2) penalizes neighboring labels if two shifted images $I(\mathbf{x} + \mathbf{s}_a)$ and $I(\mathbf{x} + \mathbf{s}_b)$ are not similar near this seam. Then the energy function (1) is optimized using multi-label graph-cuts technique [5]. For more information of MRF-based methods, refer to [24].

When solving energy function (1), utilizing all known offsets as candidate offsets may not produce pleasant results. On the one hand, some unsuitable offsets may bring in interference during the optimization process, resulting in unsatisfactory inpainting performance like structure incoherence, although a smaller energy value may be obtained in some situations. On the other hand, the computational cost of optimization (1) would not be reasonable, since the complexity of graph-cuts is $O(NK)$ where N and K are the numbers of missing pixels and offsets, respectively. To tackling the problems, selecting a few but more suitable offsets from all known offsets as candidates is a practicable way and such idea has been investigated in literature. For example, In [36], only nearby offsets were utilized. However, the performance is still not pleasant because the overall feature of the image is not considered. In He and Sun's method [24], the statistic of image features was adopted to select some dominant offsets as candidates. However, structure incoherence still appears in their results. Considering that human eye is very sensitive to structures, utilizing more structure information of the degraded image to select candidate offsets is a promising way to enhance inpainting performance. Following the idea, we propose a direction structure distribution analysis strategy to select candidate offsets and we expound it in the next section.

3. Direction structure distribution analysis

To quickly repair a degraded image and well maintain structure coherence, we adopt desired direction structure information to guide inpainting process through direction structure distribution analysis strategy. Fig. 1 gives the frame diagram of the strategy, which includes three main steps. First, super-wavelet transform is applied to generate four direction feature images. Then edge structure images are obtained via edge detection and morphological operations and gradient is utilized to measure the intensity of direction structures. On the basis, gradient variance is used to adaptively select DDS. Afterwards, similar patches are matched and offsets are respectively calculated in the selected direction structure image and non-structure image, and only a few dominant offsets are selected for energy equation optimization. In what follows, we explain each step in detail accompanied with an example.

3.1. Direction feature extraction

The Curvelet transform [42] is applied to extract direction feature information of a degraded image. Denoting the input image

as I_Y (I_Y is the Y component of a color image in YUV space), a multi-direction and multi-scale Curvelet forward transform on I_Y is formulated as:

$$Q = T^+(I_Y), \quad (3)$$

where T^+ implies the Curvelet transform and $Q = \{Q_{s,d}\}$ is the coefficient matrix sets with scale s and direction d . A multi-scale Curvelet coefficient matrix is illustrated in Fig. 2(a). The square in the center is the first scale coefficient matrix, and the squares from inside to outside are the second, third, fourth and fifth scale coefficient matrices, respectively. Different numbers of Curvelet coefficient matrix exist in all scales except the first scale where only one Curvelet coefficient matrix exists. The coefficient matrix in first scale denotes the low frequency feature, while other coefficient matrices denote high frequency feature of an image. The second to fifth scales contain 16, 32, 32 and 64 direction matrices, respectively. For convenience, we start from the 45° to number the coefficient matrix of each scale layer in a clockwise direction. Some of the 32 coefficient matrices of the fourth scale layer are labeled in Fig. 2(a). The black region is denoted by $Q_{4,1}$, followed by $Q_{4,2}, Q_{4,3}, \dots, Q_{4,32}$ in a clockwise direction. We adopt the coefficient matrices to infer the multi-direction feature of an image.

Then the Curvelet coefficient matrix $Q_{s,d}$ from the second to fifth scale layers (i.e., $s = 2, \dots, 5$) is partitioned into four sets according to four directions, as shown in Fig. 2(b), where Z_1, Z_2, Z_3 and Z_4 denotes the sets of $0^\circ, 45^\circ, 90^\circ$ and 135° Curvelet coefficient matrices, respectively. The set Z_1 does not only include the features exactly at 0° or horizontal direction of an image, but regions ranging from -22.5° to 22.5° and from 157.5° to 202.5° , and similar for other three sets. On this basis, the direction feature image A_n ($n = 1, 2, 3, 4$) on the n -th direction can be obtained by

$$A_n = T^-(H_n(Q)), \quad (4)$$

where the size of A_n equals to the size of I_Y , T^- denotes Curvelet inverse transform, and $H_n(Q)$ is defined as

$$H_n(Q) = \begin{cases} Q_{s,d}, & \text{if } Q_{s,d} \in Z_n \text{ or } s = 1 \\ 0, & \text{otherwise.} \end{cases} \quad (5)$$

Fig. 3 gives an example of four direction feature images based on A_n . It should be noted that if Curvelet transform is conducted on the degraded image Fig. 3(b), the extracted four feature images are similar to Fig. 3 except the missing region. Since we only apply the known information for the subsequent procedures, there is no difference between applying Curvelet transform on original image or degraded images. Besides, the boundary of missing region would bring the edge information with Curvelet transformation. To eliminate this interference, we could multiply A_n with a mask slightly bigger than the degraded region. From Fig. 3(c), we can observe that only horizontal direction features are prominent

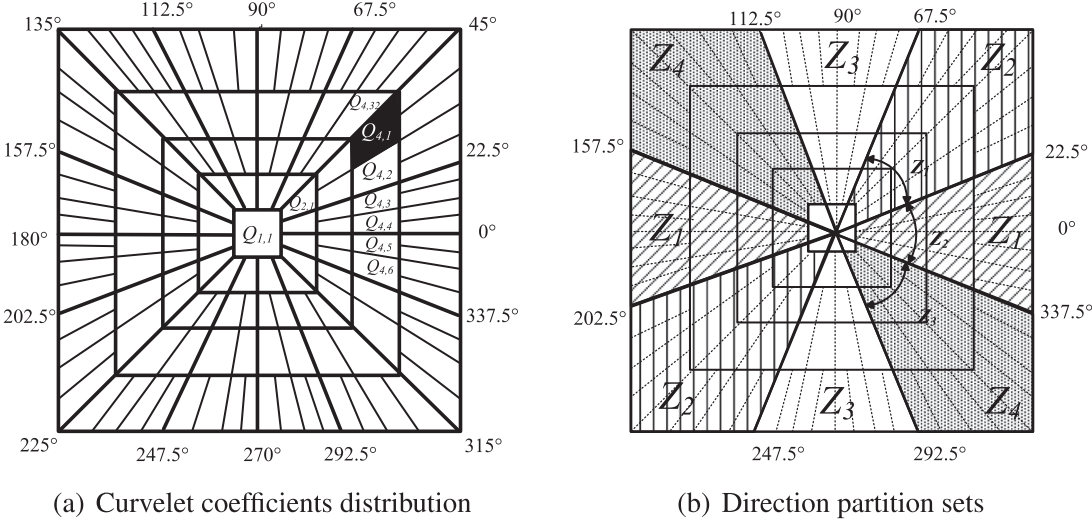


Fig. 2. Sketch of the partition of Curvelet coefficient and direction.

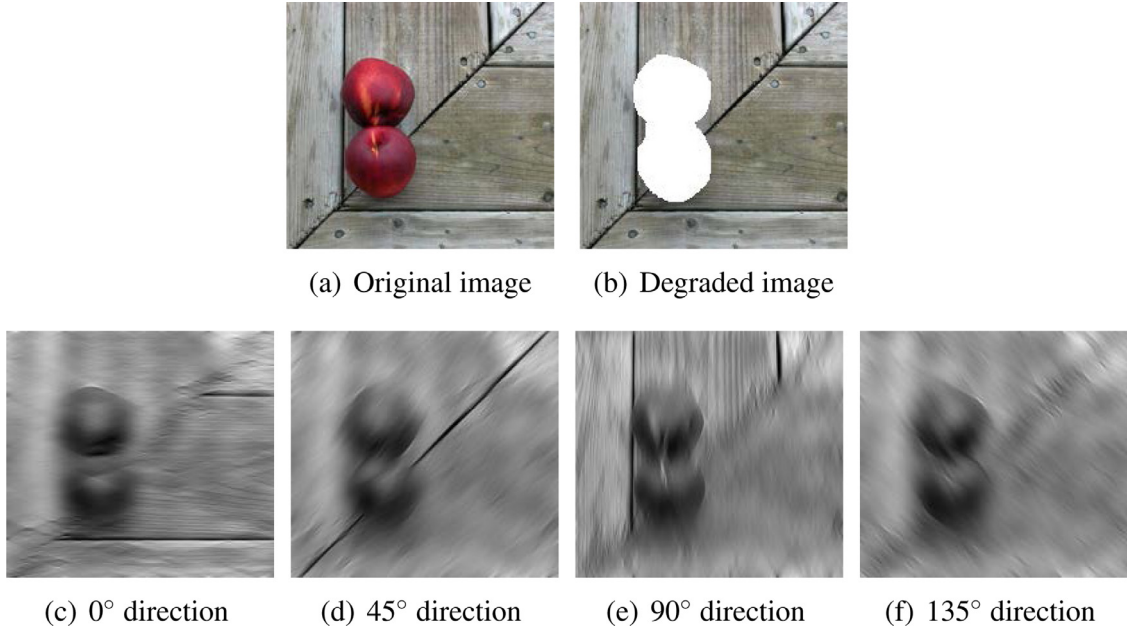


Fig. 3. An example of direction feature extraction.

in 0° direction feature image while other direction features are insignificant. Similar phenomena can be observed from other three images. The direction feature extraction procedure is similar to our previous work [33]. However, the purposes are significantly different. In the previous work, the multi-direction features were utilized to construct sparse representation constraint equation in order to make the sparse represent results more sharp, while in this work it is applied to extract multi-direction edge information, aiming to divide the degraded image into different parts for further procedures.

3.2. Desired structure feature selection

Generally speaking, only a part of direction structures are helpful for image inpainting task. For example, for the degraded image in Fig. 3(b), the desired direction structures are those at 45° and 90° directions. Moreover, the DDS usually have visible characteristic around the fill-front. Based on this observation, we adaptively select DDS for inpainting task, which works as follows.

It can be seen from Fig. 3 that four direction feature images $A_n (n = 1, 2, 3, 4)$ obtained by (4) can well reflect the direction features of 0°, 45°, 90° and 135°. Usually, direction structure is distinct from neighboring information; hence, we adopt gradient to describe the intensity of direction structure. The direction gradient magnitude image I_g^n of A_n is generated by

$$I_g^n(\mathbf{x}) = \sqrt{(G_x^{A_n}(\mathbf{x}))^2 + (G_y^{A_n}(\mathbf{x}))^2}, \quad (6)$$

where $G_x^{A_n}(\mathbf{x})$ and $G_y^{A_n}(\mathbf{x})$ are the horizontal and vertical gradient at position \mathbf{x} of A_n , which are respectively calculated by convolving direction feature image A_n with discrete gradient operators $[-0.5, 0, 0.5]$ and $[-0.5, 0, 0.5]^T$. Four direction gradient magnitude images I_g^n of Fig. 3(c) - Fig. 3(f) are presented in Fig. 4(a). To distinctly make out the strength of desired direction, Fig. 4(a) is shown with pseudo-color, that is, the minimum value and maximum value are respectively displayed with white and red color.

Meanwhile, we adopt canny and expansion operators on A_n to obtain more plentiful edge information and the direction edge

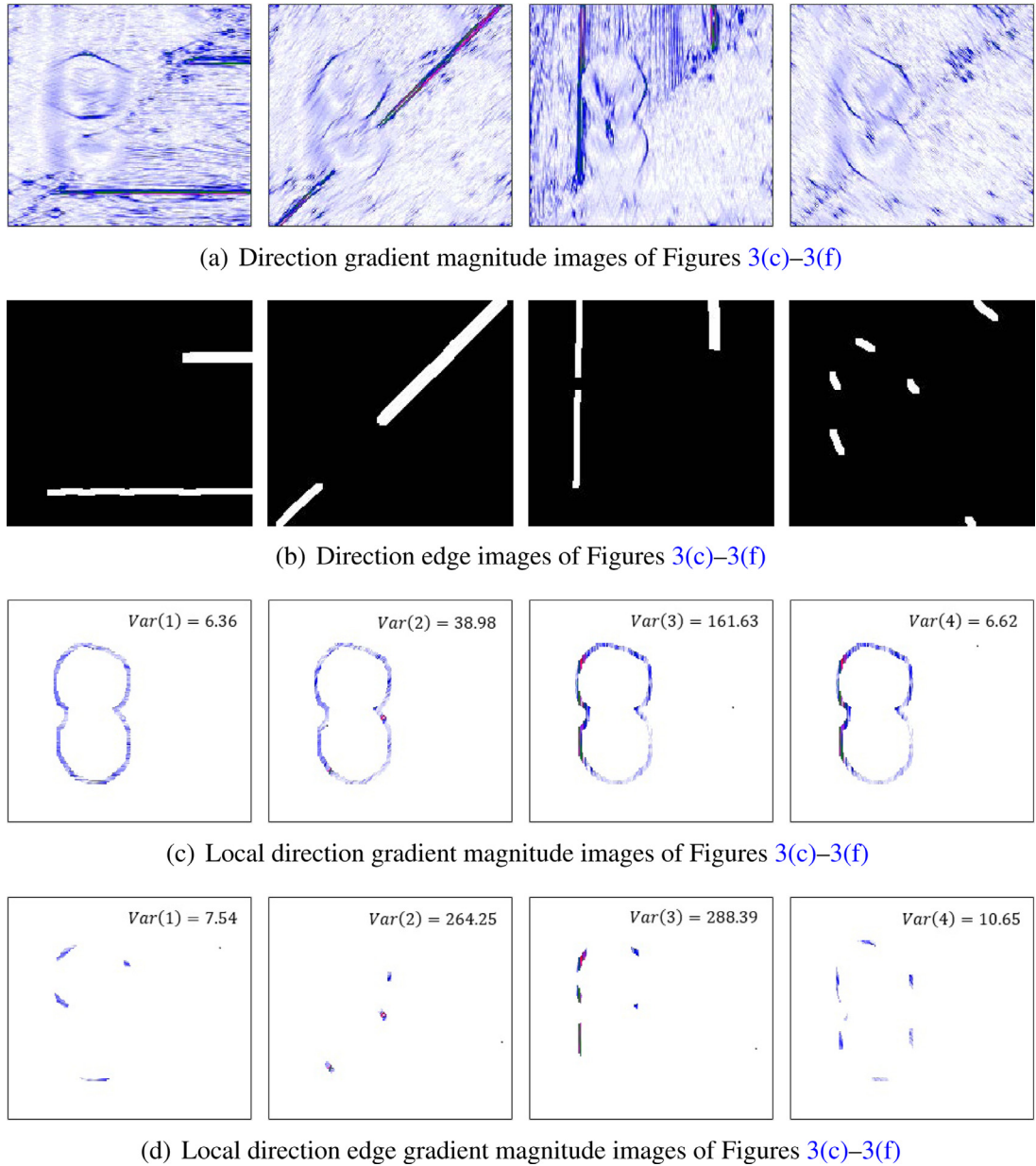


Fig. 4. Desired direction structure selection for Fig. 3.

images I_d^n can be defined as

$$I_d^n(\mathbf{x}) = \begin{cases} 1, & \text{if } \mathbf{x} \text{ locates at edge region} \\ 0, & \text{otherwise.} \end{cases} \quad (7)$$

The four direction edge images of Fig. 3 are given in Fig. 4(b). From Fig. 4(a) and Fig. 4(b), we can see that different direction feature images have different direction strong coherent edges. Furthermore, according to human eye visual requirement, we only favor the direction structures adjacent to fill-front being propagated into the missing region in order to maintain structure coherence. For the example in Fig. 3, only 45° and 90° direction features should be applied to guide the inpainting process and propagated into the missing region, while the direction feature of 0° should not be applied. To distinguish which direction feature is really useful, we further define local direction gradient magnitude I_{gs}^n by

$$I_{gs}^n = I_g^n \cdot F_L, \quad (8)$$

where $F_L = M \cdot \Omega^L$; M is the target mask and Ω^L is a neighboring known mark. M and Ω^L are respectively defined as

$$M(\mathbf{x}) = \begin{cases} 0, & \text{if } \mathbf{x} \in \Omega \\ 1, & \text{otherwise.} \end{cases} \quad (9)$$

$$\Omega^L(\mathbf{x}) = \begin{cases} 1, & \text{if } d(\mathbf{x}, \partial\Omega) < \delta \\ 0, & \text{otherwise.} \end{cases} \quad (10)$$

where δ is the distance threshold. If δ is too small, the local direction gradient magnitude is not robust. If the value is too large, other direction interference will be introduced. The local direction gradient magnitude with different δ values for Fig. 4 is listed in Table 1. According to the table, the value 5 seems to be appropriate as it well satisfies our requirements, that is 45° and 90° direction features should be applied while the others should not. Thus, δ is set to 5 in our implementation to select desire structures for guiding inpainting process.

Table 1

Local direction gradient magnitude with different δ in Fig. 4.

	0°	45°	90°	135°
$\delta = 2$	2.73	402.40	112.53	8.75
$\delta = 5$	7.54	264.25	288.39	10.65
$\delta = 8$	6.17	201.84	309.98	9.94
$\delta = 10$	6.61	169.50	307.91	9.46

The local direction gradient magnitude images and the variance values are given in Fig. 4(c). According to the figures, the variance values of 45° and 90° are much larger than the values of 0° and 135° . Although the 45° and 90° structures are desired for completing missing structures, using variance value to select desired direction structure is not significant because the variance value of 45° is less than the value of 90° in a large degree. Therefore, we further uses the points located at edge region of direction gradient magnitude image I_{gs}^n , named as local direction edge gradient magnitude image $I_{gs_d}^n$, to calculate the variance, and $I_{gs_d}^n$ is defined as

$$I_{gs_d}^n = I_{gs}^n \cdot I_d^n, \quad (11)$$

where I_d^n is defined as in (7). Images $I_{gs_d}^n$ and their variance values are given in Fig. 4(d). We can see that the images I_d^n with DDS (i.e., 45° and 90° structures) have much larger variance value than the others, and the variance difference between 45° and 90° is small. Therefore, the variance value of $I_{gs_d}^n$ can reflect the distribution of DDS, that is, the higher the variance value is, the more likely its direction structure is DDS. To automatically and adaptively select DDS, the following rule is applied,

$$\frac{\text{Var}(n)}{\min\{\text{Var}(i), i \in \{1, 2, 3, 4\}\}} > \alpha \quad \& \quad \frac{\text{Var}(n)}{\max\{\text{Var}(i), i \in \{1, 2, 3, 4\}\}} > \beta, \quad (12)$$

where $n = 1, 2, 3, 4$ which represents 0° , 45° , 90° and 135° , respectively, and α and β are two threshold setting as 10 and 0.8 in our implementation. When the variance $\text{Var}(n)$ satisfy the above condition, the pixels at direction edge region of image I are chosen as DDS. There is one exception that when the difference between any two variance values is quite small, the rule (12) will not be satisfied. For this circumstance, all the four direction structure are chosen as DDS. We denote the image consisting of DDS as I_s^n with $n \in \{1, 2, 3, 4\}$.

Another example is given in Fig. 5. From Figs. 5(e) we can see that the variances of four local direction gradient magnitude images are not diacritical enough, although the variance of horizontal directional local gradient magnitude is larger than others. However, the variance of local direction edge gradient magnitude images are much more distinguishable. According to (12), the pixels at 0° direction edge region of I will be chosen as DDS, which is consistent with human intuition in Fig. 5(a). In brief, we adopt the variance of local direction edge gradient magnitude image to describe the direction structure distribution and adaptively select DDS. We test the method on hundreds of natural images and obtain similar results.

3.3. Candidate offsets selection

In this procedure, we first separately match similar patches for I_s^n and non-structure image I_{ns} to obtain their offsets, where $I_s^n = I \cdot I_d^n$ and $I_{ns} = I / \bigcup\{I_s^n, n = 1, 2, 3, 4\}$. Specifically, for each patch $P(\mathbf{x})$ in direction edge image I_s^n in known region, we compute its offset to its most similar patch, that is,

$$S_n(\mathbf{x}) = \underset{\mathbf{s}}{\operatorname{argmin}} \|p(\mathbf{x} + \mathbf{s}) - p(\mathbf{x})\|^2, \quad \text{s.t. } |\mathbf{x}| > \tau, \quad (13)$$

where $n \in \{1, 2, 3, 4\}$; $\mathbf{s} = (u, v)$ is the 2-d coordinates of the offset; and the threshold τ is to preclude nearby patches which is set to 8 in our implementation. The offset for patch in I_{ns} is calculated in the similar way and we denote it as S_5 ¹. To efficiently compute $S_n, n \in \{1, 2, \dots, 5\}$, traditional kd-tree method is applied to find the nearest-neighbor field additionally rejecting any patch that disobeys the constraint in the search procedure. Moreover, considering the local similarity of an image, the search region is adaptively determined according to the size of missing region, that is, the matching procedure is performed in a square that is three times larger than the maximal width and height of bounding box of the hole. In most cases, if the structures or other objects are not shown in local search region, we can assume the structures or other objects may not exist in the missing region, which complies with human eye requirement.

Then for direction offset $S_n, n \in \{1, 2, 3, 4\}$, we calculate their statistics by a 2-d histogram, that is,

$$h(u, v) = \sum_{\mathbf{x}} \delta(S_n(\mathbf{x}) = (u, v)) \quad (14)$$

where $\delta(\cdot)$ is 1 when the argument is true and 0 otherwise. We pick out the K_1 highest peaks of this histogram which correspond to K_1 dominant DDS. Considering the non-structure image may contain useful textures, the above method is also utilized for offset S_5 and K_2 highest peaks are picked out. In this procedure, the calculations of direction structure offsets statistics are separately conducted in different structure parts so that no inference would be caused by other texture information. Therefore, even the known region does not contain enough desired structures, these useful structures can still be picked out. In our implementation, 60 candidate offsets are chosen in total. Specifically, if only one DDS image is selected according to (12), we set $K_1 = 40$ and $K_2 = 20$. If two DDS images are selected, we set $K_1 = 20$ and $K_2 = 20$. If three DDS images are chosen, we set $K_1 = 15$ and $K_2 = 15$. If four DDS images are selected, we set $K_1 = 10$ and $K_2 = 20$.

3.4. Algorithm analysis

By incorporating direction structure distribution analysis strategy into the framework of MRF-based algorithm, our proposed algorithm is developed. The structure of the proposed method is analogous to He's method [24], however, the two methods differ significantly in the calculation of candidate offsets. He's method calculates candidate offsets in the original image, which would introduce structure incoherence in the inpainted image. On the contrary, our method automatically selects candidate offsets according to the characteristics of the neighboring region of the target region via direction structure distribution analysis procedure, which is able to better maintain structure incoherence and therefore enhance inpainting performance.

The computational complexity of our method is reasonable. Compared with He's method, our method uses Curvelet transform to extract direction feature, which increases computational complexity. However, our method decreases computational complexity in the similar patches matching step because our method matches similar patches only in local structure or non-structure regions rather than in whole image as in He's method. Therefore, the computational complexity of our method is comparable to He's method. Compared to other MRF-based algorithms, the mainly complexity difference is determined by the number of offsets for solving energy function using graph-cuts. Generally, the computational complexity of graph-cuts is $O(NK)$, where N is the number

¹ For four structure images, the offsets are denoted as $S_1(\mathbf{x}), S_2(\mathbf{x}), S_3(\mathbf{x})$ and $S_4(\mathbf{x})$. To unify the denotations, we denoted the offsets for non-structure image as $S_5(\mathbf{x})$. Hence, the offsets can be denoted as $S_n, n \in \{1, 2, \dots, 5\}$.

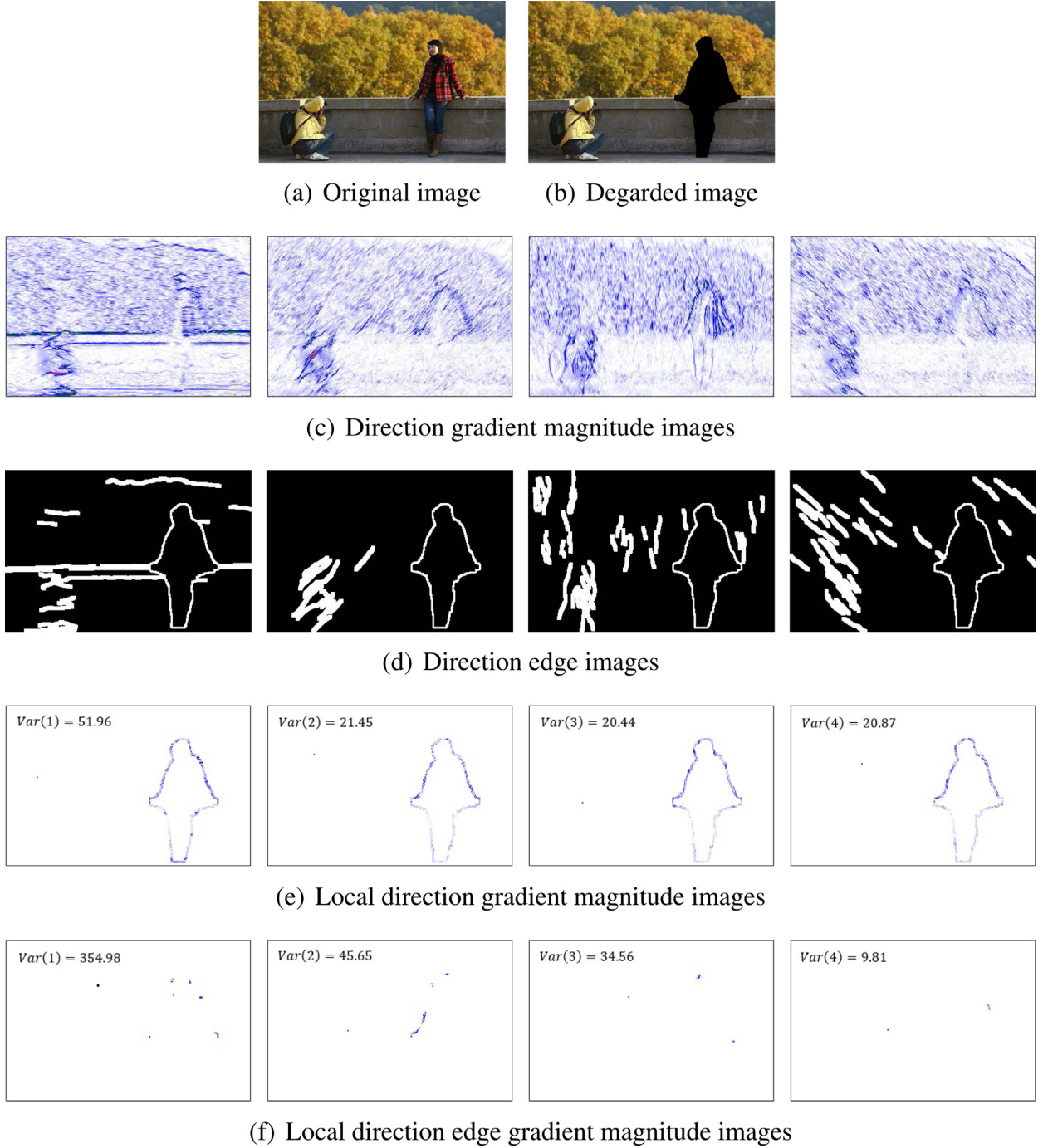


Fig. 5. Another example of desired direction structure selection.

of missing pixels and K is the number of labels or offsets. When all possible labels are used like Pritch's Shift-map approach [40], K will be huge, resulting in a large computational cost. For example, for a low resolution image with a size of 100×100 , K is of the order of 10^4 . To the contrary, we elaboratively select only a few candidate offset for solving energy function, which sharply reduce computation time. In the next section, we will experimentally validate the effectiveness and efficiency of our method by inpainting several images with different features.

4. Experimental results

In this section, the performance of the proposed method is first evaluated on inpainting various degraded images and compared

against seven state-of-the-art MRF-based methods and two state-of-the-art matching-based methods. Then, the limitations of proposed method are experimentally discussed. All the experiments are conducted on the platform is 4.0 GHz CPU, 16GB RAM and MATLAB.

4.1. Algorithm setting

There are some parameters need to be set in the proposed algorithm, including threshold δ in (10), thresholds α and β in (12), threshold τ in (13), and K_1 and K_2 in candidate offsets selection step. The parameter δ determines the region for calculating variance value $Var(n)$ in (12), and a small value is preferable. The set of parameters α and β is related to δ . Once δ is set, α and β require a careful set because they determine whether a direc-

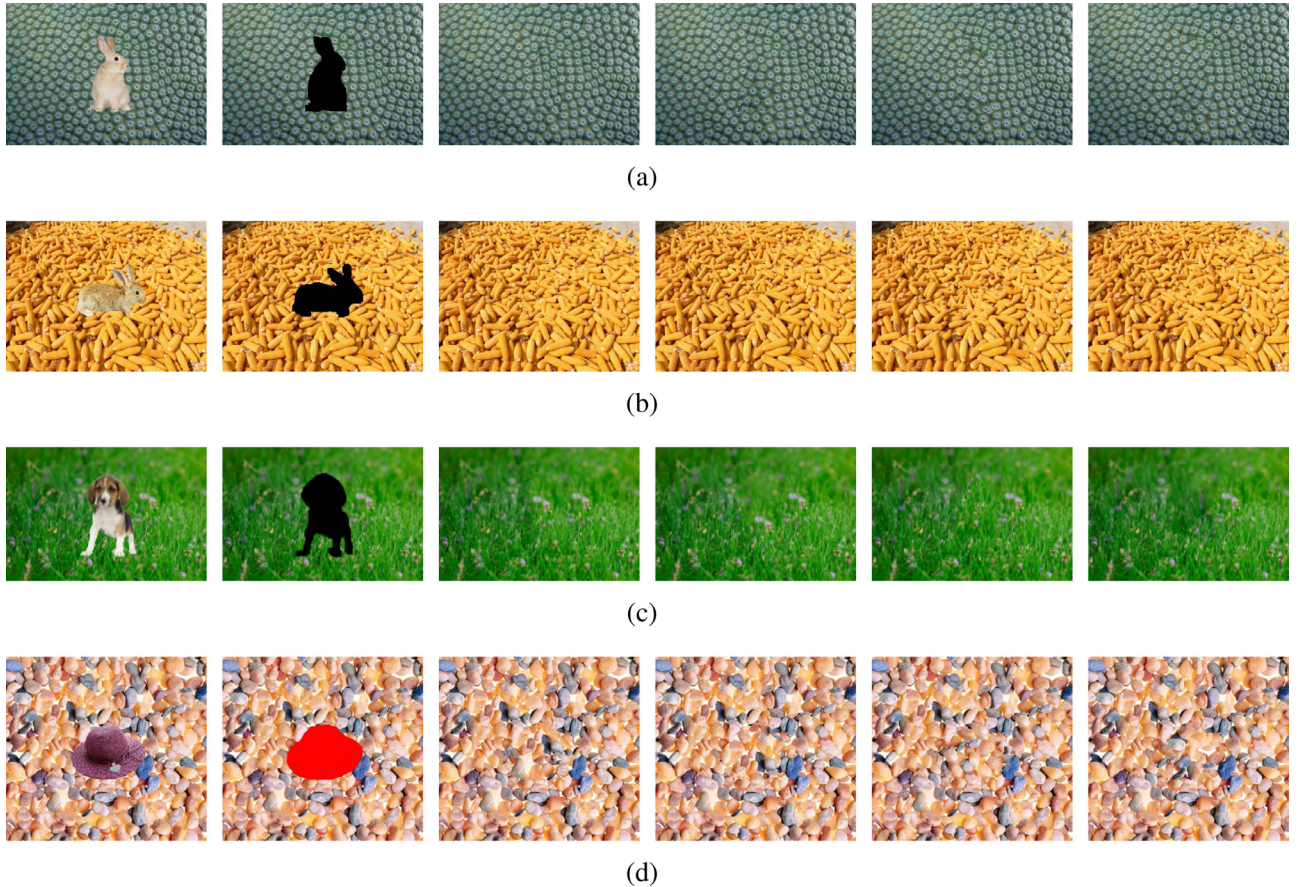


Fig. 6. Performance comparisons with MRF-based methods on inpainting texture images. For each row, the columns from left to right are the original image, degraded image, inpainted results of Pritch's [40], Liu's [36], He's [24] and our proposed methods, respectively.

tion structure is DDS and further influences the structure coherence of the inpainted images. We use a statistic inference procedure to set their values. Specifically, for a given degraded image, according to vision observation, we know which direction structure should be used for selecting offsets and then we set proper values for α and β that satisfies the requirement. We repaired hundreds of degraded images with different direction structure requirements and gets the proper values of α and β for each images. According to all the proper values, we set α to 10 and β to 0.8 in our experiments. The parameter τ is applied to eliminate self similarities in the patch matching, and it is set to 8 which is the same as He's method [24]. K_1 and K_2 determines the numbers of offsets selected from each structure image and non-structure image. The total number 60 of candidate offsets is applied which is the same as He's method [24], and we divide them almost equally into structure and non-structure parts via K_1 and K_2 . For the compared algorithms, the settings as in their original papers are applied.

4.2. Comparisons with MRF-based methods

Although our method mainly focuses on inpainting structure images, it does not mean the algorithm can not well inpaint texture images. Here, we first conduct experiments on inpainting texture images and compare our method with three state-of-the-art MRF-based methods, including Pritch's [40], Liu's [36], and He's [24] methods. The results are presented in Fig. 6, with PSNR, SSIM [50], and computation time listed in Table 2, Table 3 and Table 4. According to Fig. 6, we can see that our method can produce competitive inpainted results on texture images, which indicates that although there are no visible direction structures in these tex-

Table 2
PSNR (in dB) comparisons with MRF-based methods on inpainting texture images.

	Pritch's [40]	Liu's [36]	He [24]	Proposed
Fig. 6(a)	27.0219	27.4793	26.6383	27.5478
Fig. 6(b)	24.4339	24.1883	24.6365	24.7172
Fig. 6(c)	24.1210	24.5887	24.4609	25.2239
Fig. 6(d)	22.2696	23.0023	22.9610	23.2319

Table 3
SSIM comparisons with MRF-based methods on inpainting texture images.

	Pritch's [40]	Liu's [36]	He [24]	Proposed
Fig. 6(a)	0.9251	0.9323	0.9281	0.9357
Fig. 6(b)	0.9220	0.9250	0.9254	0.9270
Fig. 6(c)	0.8899	0.8913	0.8878	0.8995
Fig. 6(d)	0.9132	0.9215	0.9185	0.9198

Table 4

Computation time (in seconds) comparisons with MRF-based methods on inpainting texture images.

	Pritch's [40]	Liu's [36]	He [24]	Proposed
Fig. 6(a)	218.5	18.7	8.1	8.4
Fig. 6(b)	233.8	12.2	8.5	8.4
Fig. 6(c)	296.7	8.7	7.37	3.5
Fig. 6(d)	242.7	28.7	14.1	17.9

ture images, our proposed method can still obtain suitable candidate offsets for image completion. Table 2 shows that the proposed method achieves the largest PSNR values on four images. Table 3 shows that the proposed method achieves the largest SSIM

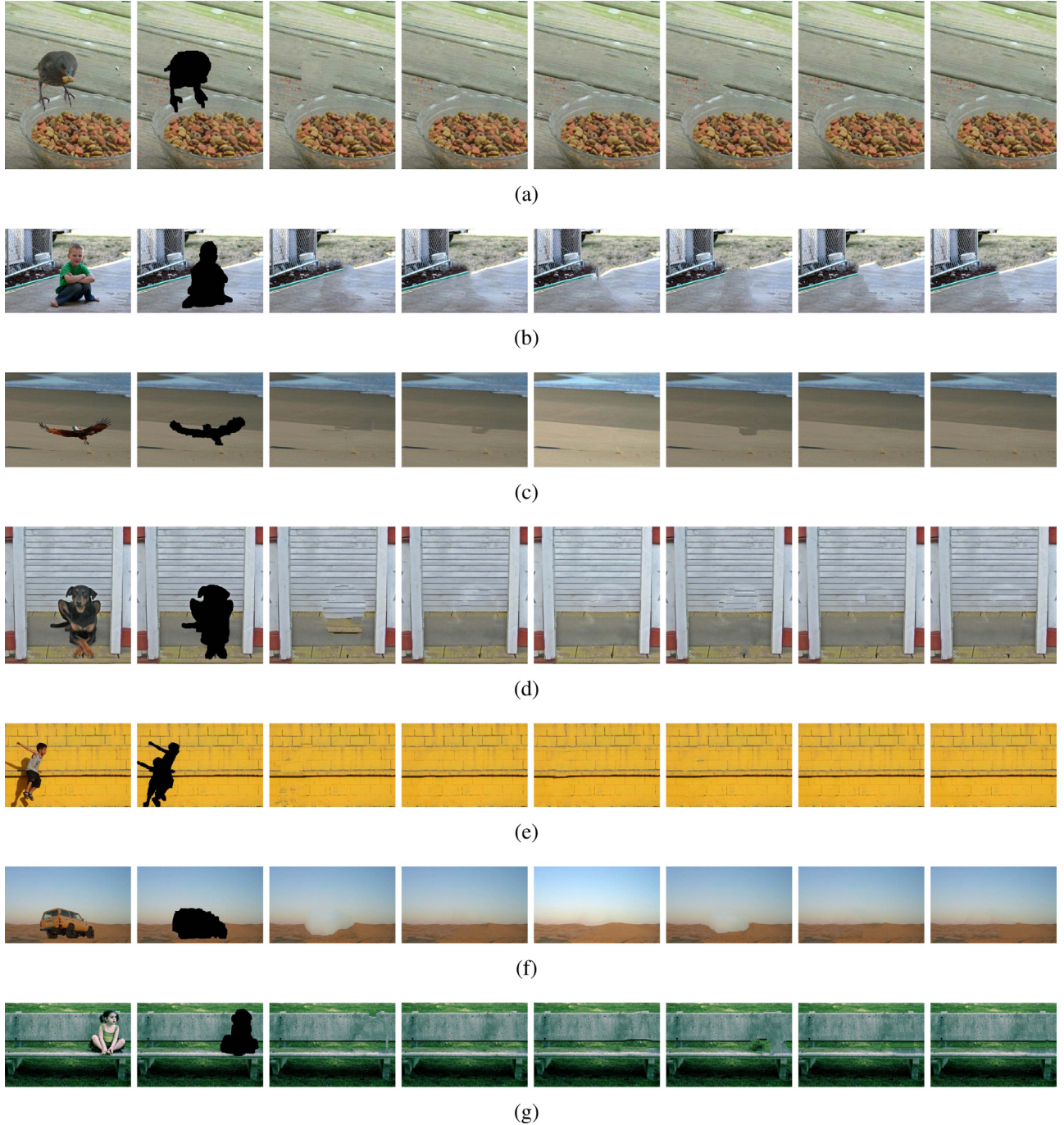


Fig. 7. Performance comparisons with MRF-based methods on inpainting structure degraded images. For each row, the columns from left to right are the original image, degraded image, inpainted results of Pritch's [40], Barnes's [2], Darabi's [14], Liu's [36], He's [24] and our proposed methods, respectively.

values on three images except the fourth one. Table 4 shows that the computation time of our method is less than Pritch's and Liu's methods, and comparative to He's method, which indicates the efficiency of our method.

To verify the performance of maintaining structure coherence, the proposed method is compared with Pritch's [40], Barnes [2], Darabi's [14], Liu's [36], and He's [24] methods. Serval degraded images and the repaired results are shown in Fig. 7, with the computation time listed in Table 5². From the third column of Fig. 7, we can see that Pritch's method can not well maintain structure

coherence, even introduce wrong fill phenomenon. The structure incoherence appears in Barnes's results, as shown in Fig. 7(b) and Fig. 7(c). For Darabi's results, structure incoherence also appears and the inpainted structures are curved, as shown in Fig. 7(a), Fig. 7(e) and Fig. 7(g). Liu's method applies the neighboring offsets to be candidate labels and achieve relatively better repaired results than those of Pritch's method. However, the method still can not well maintain structure coherence, as shown in the sixth column of Fig. 7. He's method adopts the statistics of offsets between similar patches and therefore it can produce relatively better in-

² Since the original images of structure degraded images are not available, PSNR and SSIM can not be calculated. Besides, we use the tool Content-Aware Fill in

Photoshop to implement Barnes's method, so the computation time for Barnes's method can not be provided.

Table 5

Computation time (in seconds) comparisons with MRF-based methods on inpainting structure degraded images.

	Pritch's [40]	Darabi's [14]	Liu [36]	He [24]	Proposed
Fig. 7(a)	588.1	495.6	83.1	21.9	30.4
Fig. 7(b)	401.2	462.2	202.4	44.3	30.7
Fig. 7(c)	673.1	505.8	37.4	20.5	44.1
Fig. 7(d)	717.5	611.2	168.1	17.2	38.9
Fig. 7(e)	321.3	522.8	87.1	14.3	19.9
Fig. 7(f)	400.2	341.8	159.5	23.9	20.5
Fig. 7(g)	631.9	526.6	102.5	33.4	13.9

Table 6

Computation time (in seconds) comparisons with He's method on inpainting the images with small quantity of known structures.

	Fig. 8(a)	Fig. 8(b)	Fig. 8(c)	Fig. 8(d)	Fig. 8(e)	Fig. 8(f)
He's [24]	10.4	10.5	26.8	10.9	32.3	29.7
Proposed	15.7	9.7	22.6	17.7	22.3	37.8

painting results than former methods. However, on Fig. 7(b) and Fig. 7(d), the results seem to be unpleasant as the structure coherence is not maintained. The reason is He's method does not distinguish the patches locating at structures or not. From the last column, we can see that our proposed method faithfully recovers the structures and the results satisfy human eye visual requirement. Table 5 also indicates the high efficiency of the proposed method.

Considering that both He's [24] and our proposed method adopts a few dominant offsets for inpainting task, a further comparison between the two methods is conducted. To clearly demonstrate the advantage of the proposed approach, both the inpainted results and the dominant offsets distributions on inpainting the images with small quantity of known structures are presented in Fig. 8, with the computation time are listed in Table 6. From the fourth column of Fig. 8, we can see that for He's method, the offsets do not distribute along the desired structure features. Therefore, the structure coherence is not well maintained, as shown in the third column. Contrarily, our method maintains the structure coherence very well. It is because our method separately calculates the offsets in the non-edge image and the desired direction edge image(s) which is(are) adaptively determined. The last column indicates that our method captures desired direction distribution, which helps to maintain structure coherence. Moreover, Fig. 8(f) shows that our method can well inpaint images with repetitive structures. According to the fourth and sixth columns of Fig. 8(e), we can see that local search method can generate better offsets than whole search method as in He's algorithm. Table 6 indicates that both He's and our methods have high efficiencies because the two methods adopt only a few offsets to solve energy function. The slight computation time difference is due to the different iteration numbers applied. The inpainting results and the computation time indicate that our direction structure distribution analysis strategy can improve the inpainting performance of MRF-based methods without increasing computational complexity.

To further investigate the performance of our proposed method, an experiment compared with two recently proposed MRF-based algorithms, i.e., Ružić's method [41] and Ghorai's [20] method are conducted. Ružić's method considered the structural context of image blocks in patch selection, while the group based patch selection and patch refinement were jointly used in Ghorai's method. The results are illustrated in Fig. 9 and Fig. 10. The red rectangles in Fig. 9 show that our method can produce better results in terms of structure completion and texture synthesis than Ružić's method, while the red rectangles in Fig. 10 reflect that our method can better inpaint images with repetitive structure than Ghorai's

Table 7

PSNR (in dB) comparisons with matching-based methods on completing large missing region.

	Fig. 11(d)	Fig. 11(e)	Fig. 11(f)
Xu's [52]	27.3862	30.9407	43.2181
Li's [33]	27.4602	32.3097	43.6573
Proposed	27.3702	33.2629	44.8246

Table 8

SSIM comparisons with matching-based methods on completing large missing region.

	Fig. 11(d)	Fig. 11(e)	Fig. 11(f)
Xu's [52]	0.9451	0.9849	0.9919
Li's [33]	0.9432	0.9875	0.9920
Proposed	0.9430	0.9888	0.9937

Table 9

Computation time (in seconds) comparisons with matching-based methods on completing large missing region.

	Xu's [52]	Li's [33]	Proposed
Fig. 11(a)	3910.1	720.3	11.7
Fig. 11(b)	2617.4	563.1	12.1
Fig. 11(c)	3137.2	962.6	13.7
Fig. 11(d)	591.1	138.1	7.4
Fig. 11(e)	1585.8	63.6	10.7
Fig. 11(f)	3156.8	69.9	16.0

method. According to the results, we can conclude that the proposed method is superior to the compared MRF-based methods.

4.3. Comparisons with matching-based methods

The matching-based and MRF-based inpainting methods are much appropriate for completing large missing region. Therefore, this experiment aims to validate the performance of our proposed method on such kind of inpainting task. Two state-of-the-art matching-based algorithms, i.e., Xu's method [52] and our previous work [33] (labeled as Li's hereafter) are chosen as comparative methods. In Xu's method, patch structure sparsity and sparse representation were proposed for patch priority and patch representation. In Li's method, the color-direction patch sparsity was devised for maintain structure coherence. The inpainting results are presented in Fig. 11, with PSNR, SSIM and computation time are listed in Table 7, Table 8³ and Table 9, respectively.

From Fig. 11, we can see that Xu's results can not meet human eye visual requirement, where structure incoherence, neighborhood inconsistence and error accumulation phenomenon exist in the repaired region. Though Li's approach produces better inpainted results, error accumulation phenomenon exists in the repaired regions. Comparatively, our proposed approach can well maintain structure coherence and neighborhood consistence of the inpainted images, regardless of the degraded images with structure or texture missing situations. Moreover, our proposed approach greatly alleviates error accumulation phenomenon. Therefore, the proposed approach can obtain better inpainted results than the two matching-based methods. Meanwhile, the PSNR and SSIM values for Fig. 11(e) and Fig. 11(f) indicate that the proposed algorithm can well maintains structure coherence on inpainting structure images. Though the PSNR and SSIM values of our method on inpainting texture image in Fig. 11(d) are slightly smaller than those of two compared algorithms, our result has better visual effect, which still demonstrates the good performance of

³ The tables only list the values for the images that the original images are available for the calculation of PSNR and SSIM.

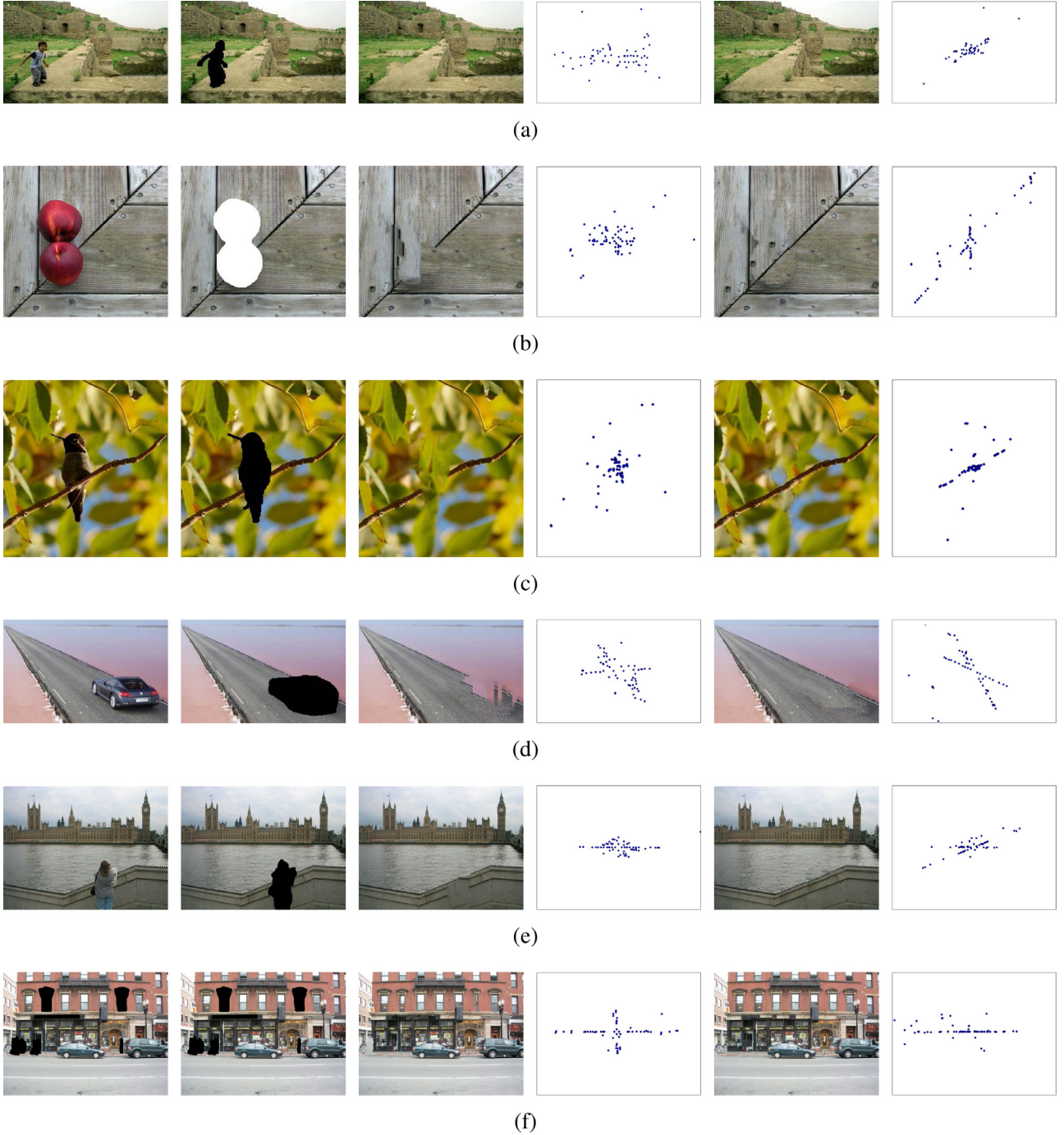


Fig. 8. Performance and offsets comparisons with He's method [24] on inpainting the images with small quantity of known structures. For each row, the columns from left to right are the original image, degraded image, the inpainted results and the offsets of He's [24] and our proposed methods, respectively.

our method. Table 9 indicates that the efficiency of our method are far higher than the compared methods. The reason is both Xu's and Li's methods only fill one patch at one iteration, while our method adopts energy function to solve the completion problem and it is not an iterative method.

4.4. Limitation discussion

The previous experiments verify the superiorities of our proposed method over nine state-of-the-art algorithms on repairing texture degraded images and completing structure missing images in terms of effectiveness and efficiency. However, it does not mean

that our method can maintain structure coherence on arbitrary images. Two limitations are illustrated in Fig. 12. Fig. 12(a) and Fig. 12(b) are two examples of unsuccessful object removals of our method as well as He's [24] method. For Fig. 12(a), our method basically maintains structure coherence and obtains more pleasant result than He's; however, it still does not well satisfy human eye visual requirement. As for Fig. 12(b), because all the neighboring vertical structures are covered, according to our direction structure distribution analysis scheme, only structure on 45° direction is selected to guide the inpainting process. Hence, the vertical structures can not be repaired. If some direction structure exists in the known region adjacent to the fill-front, the proposed method can

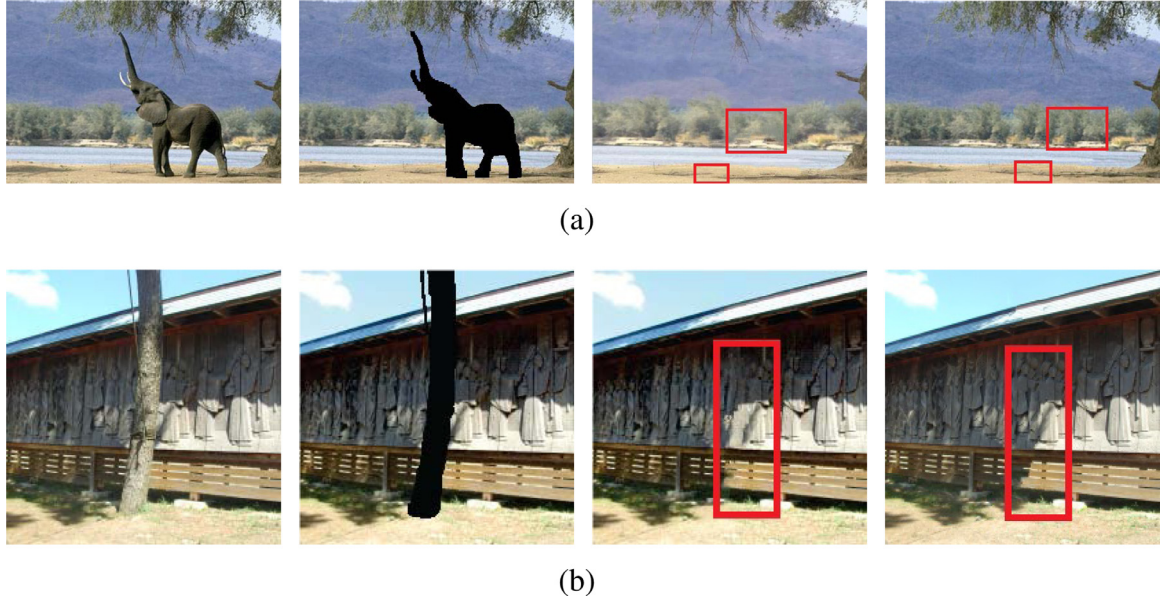


Fig. 9. Performance comparisons with Ružić's [41] method. For each row, the columns from left to right are the original image, degraded image, inpainted results of Ružić's and our proposed methods, respectively.

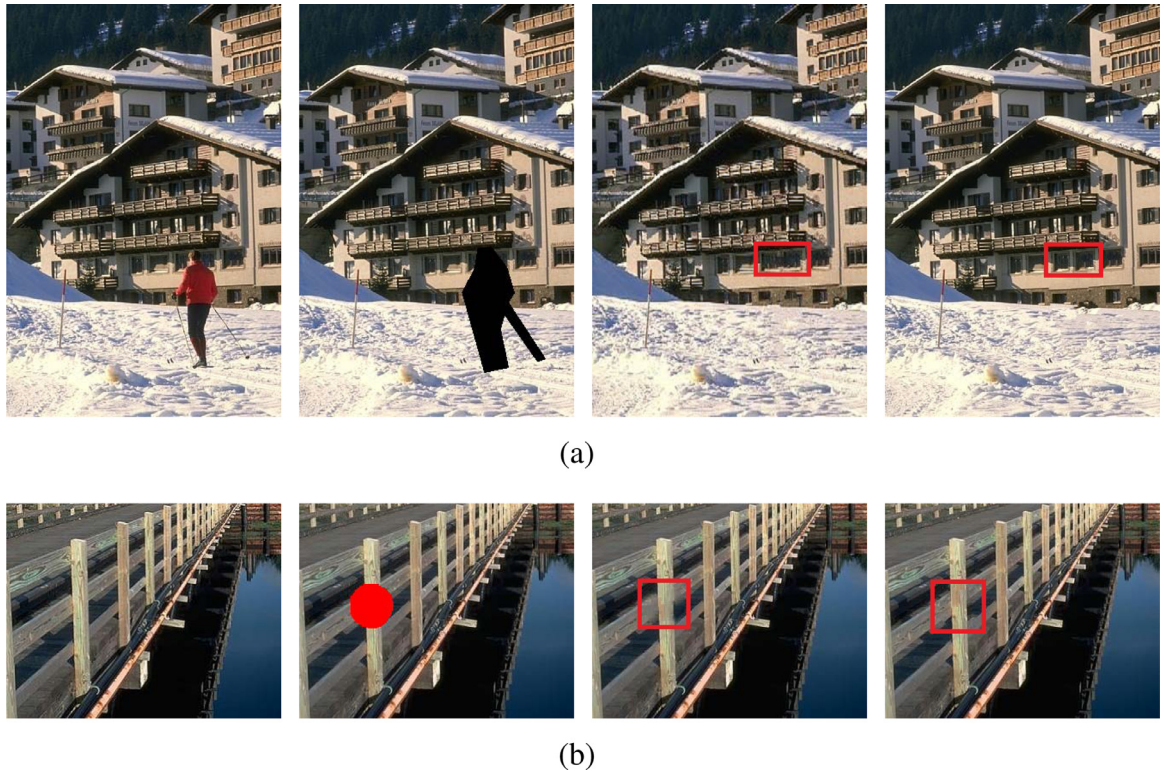


Fig. 10. Performance comparisons with Ghorai's [20] method. For each row, the columns from left to right are the original image, degraded image, inpainted results of Ghorai's and our proposed methods, respectively.

still maintain the structure coherence, as shown in Fig. 12(c). Another limitation is the performance on inpainting the images with curved structure is not so pleasant, as shown in Fig. 12(d) and Fig. 12(e). Both He's and our methods could not precisely repaired curved structure, however, our results still surpass the results obtained by He's method in a certain degree.

5. Conclusions

Considering the facts that image statistics have been proved to be essential in computer vision and human eye is sensitive to high frequency information (i.e. structures), this paper proposes a new MRF-based image inpainting algorithm particularly for maintaining

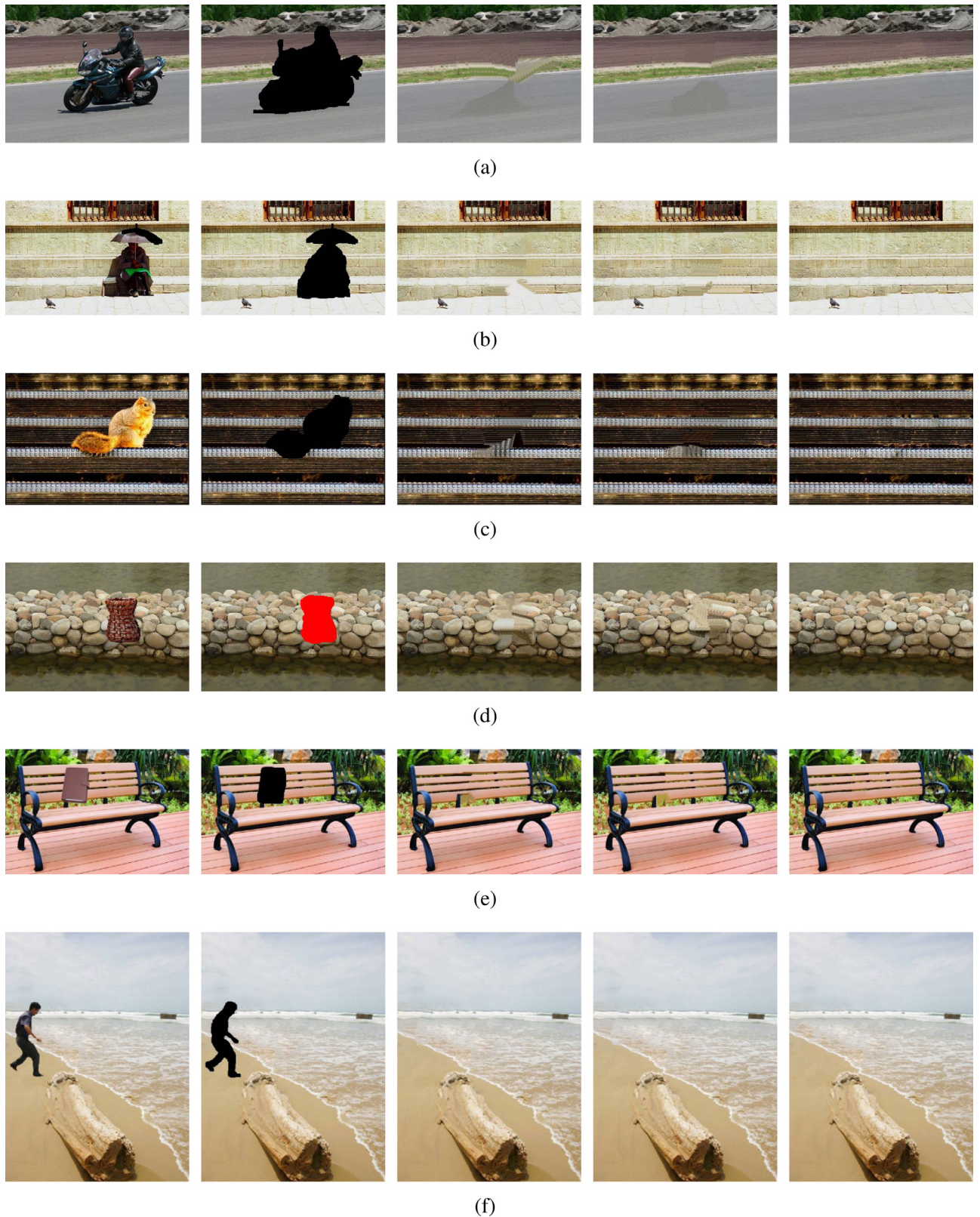


Fig. 11. Performance comparisons with matching-based methods on completing large missing region. For each row, the columns from left to right are the original image, degraded image, inpainted results of Xu's [52], Li's [33] and our proposed methods, respectively.

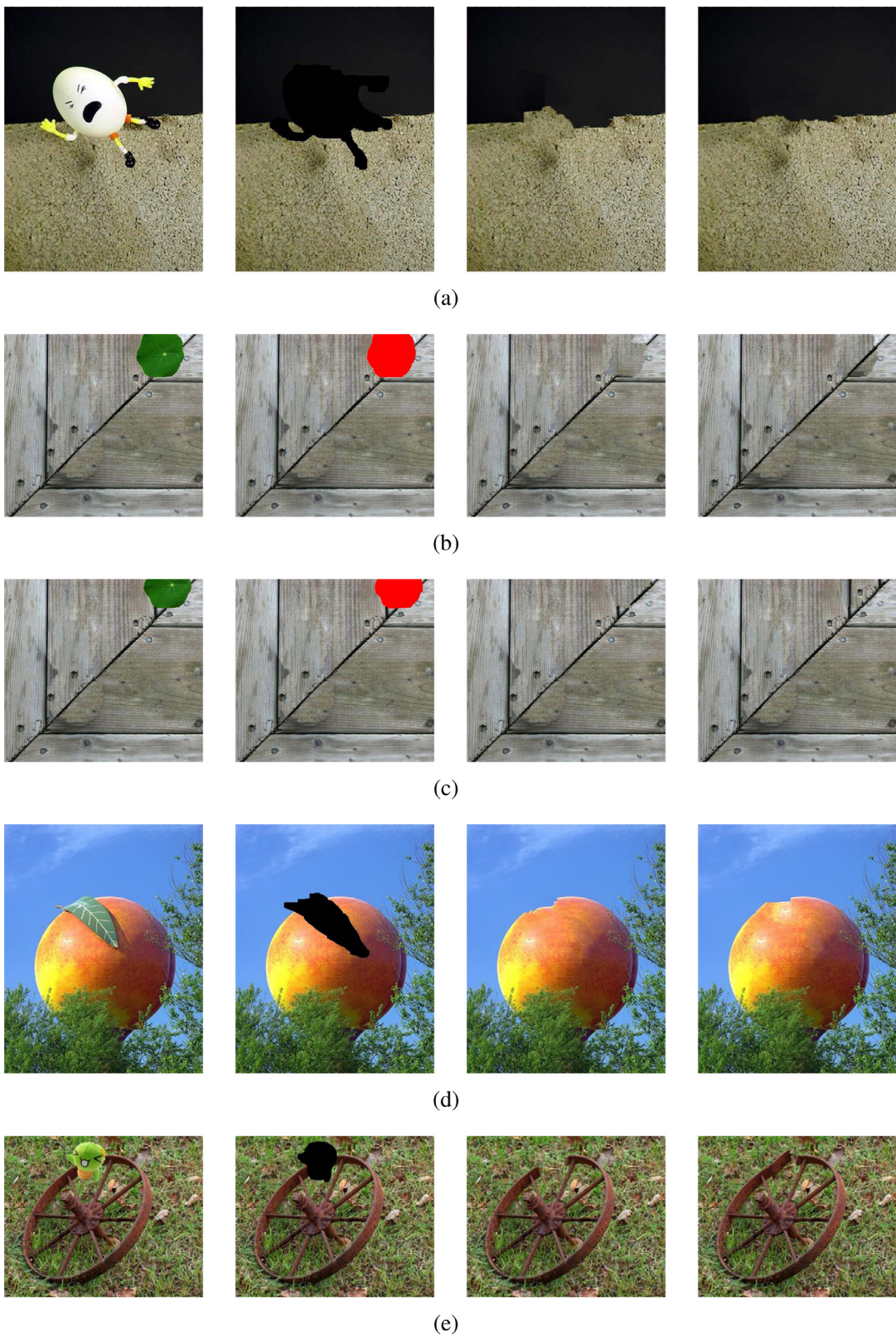


Fig. 12. Examples of the unsuccessful inpainted results of our method. For each row, the columns from left to right are the original image, degraded image, inpainted results of He's [24] and our proposed methods, respectively.

structure coherence. To legitimately and automatically choose DDS, a direction structure distribution analysis strategy is proposed. After obtaining desired direction edge image(s) and non-edge image we separately calculate statistics offsets, which gives a more reliable clue for completing degraded images. Also, the numbers of direction offsets and non-direction offsets are adaptively determined. Compared with nine state-of-the-art methods, our approach achieves better inpainting performance, that is, our method can better maintain structure coherence and satisfy human eye requirement on inpainting different kinds of degraded images, and the efficiency is higher than or competitive to the compared approaches. For the future work, the performance of our method on inpainting images with curved structure needs to be further improved and including patch geometric transformation in patch selection is a feasible way. In addition, the idea of our method can be extended for the research fields that also use image statistic such as image deconvolution, image denosing and image super-resolution.

Acknowledgements

This work was supported by the National Natural Science Foundation for Young Scientists of China (61603319, 61601385) and the Youth Science and Technology Innovation Team Cultivation Project of Southwest Petroleum University (2017CXTD010).

The authors thank Y. Liu of [36] and S. Darabi of [14] for providing the source code of their approaches which helps in developing the presented work.

References

- [1] V. Alilou, F. Yaghmaee, Application of GRNN neural network in non-texture image inpainting and restoration, *Pattern Recognit. Lett.* 62 (2015) 24–31.
- [2] C. Barnes, E. Shechtman, A. Finkelstein, D. Goldman, Patchmatch: a randomized correspondence algorithm for structural image editing, *ACM Trans. Graph.* 28 (3) (2009) 24:1–24:11.
- [3] M. Bertalmio, A.L. Bertozzi, G. Sapiro, Navier-stokes, fluid dynamics, and image and video inpainting, in: *IEEE Computer Society Conference on Computer Vision and Pattern Recognition*, 2001, pp. 355–362.
- [4] M. Bertalmio, G. Sapiro, V. Caselles, C. Ballester, Image inpainting, in: *International conference on Computer graphics and interactive techniques*, 2000, pp. 417–424.
- [5] Y. Boykov, O. Veksler, R. Zabih, Fast approximate energy minimization via graph cuts, *IEEE Trans. Pattern Anal. Mach. Intell.* 23 (11) (2001) 1222–1239.
- [6] A. Bugeau, M. Bertalmio, V. Caselles, G. Sapiro, A comprehensive framework for image inpainting, *IEEE Trans. Image Process.* 19 (10) (2010) 2634–2645.
- [7] J.F. Cai, R.H. Chan, Z. Shen, A framelet-based image inpainting algorithm, *Appl. Comput. Harmon. Anal.* 24 (2) (2008) 131–149.
- [8] R.H. Chan, Y.-W. Wen, A.M. Yip, A fast optimization transfer algorithm for image inpainting in wavelet domains, *IEEE Trans. Image Process.* 18 (7) (2009) 1467–1476.
- [9] T. Chan, J. Shen, Nontexture inpainting by curvature-driven diffusions, *J. Vis. Commun. Image Represent.* 12 (4) (2001) 436–449.
- [10] Q. Cheng, H. Shen, L. Zhang, P. Li, Inpainting for remotely sensed images with a multichannel nonlocal total variation model, *IEEE Trans. Geosci. Remote Sens.* 52 (1) (2014) 175–187.
- [11] B. Chung, C. Yim, Hybrid error concealment method combining exemplar-based image inpainting and spatial interpolation, *Signal Process. Image Commun.* 29 (10) (2014) 1121–1137.
- [12] A. Criminisi, P. Pérez, K. Toyama, Region filling and object removal by exemplar-based image inpainting, *IEEE Trans. Image Process.* 13 (9) (2004) 1200–1212.
- [13] W. Dai, E. Kerman, O. Milenkovic, A geometric approach to low-rank matrix completion, *IEEE Trans. Inform. Theory* 58 (1) (2012) 237–247.
- [14] S. Darabi, E. Shechtman, C. Barnes, D. Goldman, P. Sen, Image melding: combining inconsistent images using patch-based synthesis, *ACM Trans. Graph.* 31 (4) (2012) 82:1–82:10.
- [15] W. Dong, G. Shi, X. Li, Nonlocal image restoration with bilateral variance estimation: a low-rank approach, *IEEE Trans. Image Process.* 22 (2) (2013) 700–711.
- [16] M. Elad, J.L. Starck, P. Querre, D.L. Donoho, Simultaneous cartoon and texture image inpainting using morphological component analysis MCA, *Appl. Comput. Harmon. Anal.* 19 (3) (2005) 340–358.
- [17] J.M. Fadili, J.L. Starck, F. Murtagh, Inpainting and zooming using sparse representations, *Comput. J.* 52 (1) (2009) 64–79.
- [18] J. Fan, T. Chow, Deep learning based matrix completion, *Neurocomputing* 266 (1) (2017) 540–549.
- [19] J. Florinabel, S.E. Juliet, V. Sadasivam, Combined frequency and spatial domain-based patch propagation for image completion, *Comput. Graph.* 35 (6) (2011) 1051–1062.
- [20] M. Ghorai, S. Mandal, B. Chanda, A group-based image inpainting using patch refinement in MRF framework, *IEEE Trans. Image Process.* 27 (2) (2018) 556–567.
- [21] C. Guillemot, M. Turkan, O. Meur, M. Ebdelli, Object removal and loss concealment using neighbor embedding methods, *Signal Process. Image Commun.* 28 (10) (2013) 1405–1419.
- [22] O.G. Guleryuz, Nonlinear approximation based image recovery using adaptive sparse reconstructions and iterated denoising-part ii: adaptive algorithms, *IEEE Trans. Image Process.* 15 (3) (2006) 555–571.
- [23] D. Gupta, V. Chhajer, A. Mishra, C.V. Jawahar, A non-local mrf model for heritage architectural image completion, in: *Indian Conference on Computer Vision, Graphics and Image Processing*, 2012, pp. 61–68.
- [24] K. He, J. Sun, Image completion approaches using the statistics of similar patches, *IEEE Trans. Pattern Anal. Mach. Intell.* 36 (12) (2014) 2423–2435.
- [25] J. Huang, S. Kang, N. Ahuja, J. Kopf, Image completion using planar structure guidance, *ACM Trans. Graph.* 33 (4) (2014) 129:1–129:10.
- [26] S. Iizuka, E. Simo-Serra, H. Ishikawa, Globally and locally consistent image completion, *ACM Trans. Graph.* 36 (4) (2017) 107:1–107:14.
- [27] J. Jia, C. Tang, Image repairing: Robust image synthesis by adaptive ND tensor voting, in: *IEEE Conference on Computer Vision and Pattern Recognition*, Vol. 1, 2003, pp. 643–650.
- [28] N. Komodakis, G. Tziritas, Image completion using efficient belief propagation via priority scheduling and dynamic pruning, *IEEE Trans. Image Process.* 16 (11) (2007) 2649–2661.
- [29] P. Li, S.J. Li, Z.A. Yao, Z.J. Zhang, Two anisotropic fourth-order partial differential equations for image inpainting, *IET Image Process.* 7 (3) (2013) 260–269.
- [30] S. Li, M. Zhao, Image inpainting with salient structure completion and texture propagation, *Pattern Recognit. Lett.* 32 (9) (2011) 1256–1266.
- [31] X. Li, Patch-based image interpolation: algorithms and applications, *International Workshop on Local and Non-Local Approximation in Image Processing*, 2008.
- [32] Y. Li, L. Shen, B.W. Suter, Adaptive inpainting algorithm based on DCT induced wavelet regularization, *IEEE Trans. Image Process.* 22 (2) (2013) 752–763.
- [33] Z. Li, H. He, H. Tai, Z. Yin, F. Chen, Color-direction patch-sparsity-based image inpainting using multidirection features, *IEEE Trans. Image Process.* 24 (3) (2015) 1138–1152.
- [34] Z. Li, H. He, Z. Yin, F. Chen, A color-gradient patch sparsity based image inpainting algorithm with structure coherence and neighborhood consistency, *Signal Process.* 99 (2014) 116–128.
- [35] J. Liu, S. Zhang, W. Yang, H. Li, A fast image inpainting method based on hybrid similarity-distance, in: *International Conference on Pattern Recognition*, 2010, pp. 4432–4435.
- [36] Y. Liu, V. Caselles, Exemplar-based image inpainting using multiscale graph cuts, *IEEE Trans. Image Process.* 22 (5) (2013) 1699–1711.
- [37] X. Lu, T. Gong, P. Yan, Y. Yuan, X. Li, Robust alternative minimization for matrix completion, *IEEE Transactions on Systems, Man, and Cybernetics Part B: Cybernetics* 42 (3) (2012) 939–949.
- [38] O.L. Meur, M. Ebdelli, C. Guillemot, Hierarchical super-resolution-based inpainting, *IEEE Trans. Image Process.* 22 (10) (2013) 3779–3790.
- [39] D. Pathak, P. Krahenbuhl, J. Donahue, T. Darrell, A. Efros, Context encoders: Feature learning by inpainting, in: *IEEE Conference on Computer Vision and Pattern Recognition*, 2016, pp. 2536–2544.
- [40] Y. Pritch, E. Kav-Venaki, S. Peleg, Shift-map image editing, in: *IEEE International Conference on Computer Vision*, 2009, pp. 151–158.
- [41] T. Ružić, A. Pižurica, Context-aware patch-based image inpainting using markov random field modeling, *IEEE Trans. Image Process.* 24 (1) (2015) 444–456.
- [42] J. Starck, E. Candès, D. Donoho, The curvelet transform for image denoising, *IEEE Trans. Image Process.* 11 (6) (2002) 670–684.
- [43] J. Sun, L. Yuan, J. Jia, H. Shum, Image completion with structure propagation, in: *ACM SIGGRAPH*, 2005, pp. 861–868.
- [44] H. Takeda, S. Farsiu, P. Milanfar, Kernel regression for image processing and reconstruction, *IEEE Trans. Image Process.* 16 (2) (2007) 349–366.
- [45] A. Telea, An image inpainting technique based on the fast marching method, *J. Graph. Tools* 9 (1) (2004) 23–34.
- [46] A. Tsai, A. Yezzi, A. Willsky, Curve evolution implementation of the mumford-shah functional for image segmentation, denoising, interpolation and magnification, *IEEE Trans. Image Process.* 10 (8) (2001) 1169–1186.
- [47] H. Wang, L. Jiang, R. Liang, X. Li, Exemplar-based image inpainting using structure consistent patch matching, *Neurocomputing* 269 (2017) 90–96.
- [48] J. Wang, K. Lu, D. Pan, N. He, B. Bao, Robust object removal with an exemplar-based image inpainting approach, *Neurocomputing* 123 (2014) 150–155.
- [49] M. Wang, B. Yan, K.N. Ngan, An efficient framework for image/video inpainting, *Signal Process. Image Commun.* 28 (7) (2013) 753–762.
- [50] Z. Wang, A. Bovik, H. Sheikh, E. Simoncelli, Image quality assessment: from error visibility to structural similarity, *IEEE Trans. Image Process.* 13 (4) (2004) 600–612.
- [51] Y. Xu, L. Yu, H. Xu, H. Zhang, T. Nguyen, Vector sparse representation of color image using quaternion matrix analysis, *IEEE Trans. Image Process.* 24 (4) (2015) 1315–1329.
- [52] Z. Xu, J. Sun, Image inpainting by patch propagation using patch sparsity, *IEEE Trans. Image Process.* 19 (5) (2010) 1153–1165.
- [53] W. Xue, R. Zhang, Graph-based image completion using patch offsets and

- structure feature, in: International Conference on Graphic and Image Processing, 2014.
- [54] R. Yeh, C. Chen, T.Y. Lim, A.G. Schwing, M. Hasegawa-Johnson, M. Do, Semantic image inpainting with deep generative models, in: IEEE Conference on Computer Vision and Pattern Recognition, 2017, pp. 5485–5493.
- [55] Q. Zhang, J. Lin, Exemplar-based image inpainting using color distribution analysis, *J. Inform. Sci. Eng.* 28 (4) (2012) 641–654.
- [56] Y. Zhang, Y. Pu, J. Zhou, Two new nonlinear PDE image inpainting models, in: International Workshop on Computer Science for Environmental Engineering and EcoInformatics, 2011, pp. 341–347.